Combustion synthesis of Ce/Mg co-doped ZnO nanoparticles as a visible-light-driven photocatalyst

A. Phuruangrat[a,*], T. Thongtem[b,c], S. Thongtem[b,d]
[a]*Division of Physical Science, Faculty of Science, Prince of Songkla University, Hat Yai, Songkhla 90112, Thailand*
[b]*Materials Science Research Center, Faculty of Science, Chiang Mai University, Chiang Mai 50200, Thailand*
[c]*Department of Chemistry, Faculty of Science, Chiang Mai University, Chiang Mai 50200, Thailand*
[d]*Department of Physics and Materials Science, Faculty of Science, Chiang Mai University, Chiang Mai 50200, Thailand*

ZnO and Ce/Mg co-doped ZnO nanoparticles as a visible-light-driven photocatalyst were synthesized by combustion method. X-ray diffraction (XRD) patterns of ZnO and Ce/Mg co-doped ZnO samples were indexed to the pure phase of hexagonal wurtzite ZnO structure without impurity detection. The Raman analysis of ZnO and Ce/Mg co-doped ZnO samples showed optical phonon E_{2H}, A_1(TO), E_{2L}, E_{2H}–E_{2L}, A_1(LO) and E_1(LO) modes of wurtzite ZnO structure, including the detection of Zn−O stretching mode containing in FTIR spectra of hexagonal wurtzite ZnO. Transmission electron microscopic (TEM) images of ZnO and Ce/Mg co-doped ZnO samples showed uniform and good distribution of nanoparticles with different orientations. The photocatalysis of ZnO and Ce/Mg co-doped ZnO nanoparticles was studied through the degradation of methylene blue (MB) illuminated by visible radiation. In this research, the $Zn_{0.97}Ce_{0.015}Mg_{0.015}O$ nanoparticles have the highest efficiency of 95.16% within 150 min because of the largest specific surface area, smallest crystallite size and highest absorption capacity of visible light for active species production in degrading of MB under visible light. Photocatalytic mechanism of Ce/Mg co-doped ZnO nanoparticles in degrading MB was also proposed.

(Received December 21, 2023; Accepted March 19, 2024)

Keywords: Ce/Mg co-doped ZnO nanoparticles, Visible-light-driven photocatalyst, Wastewater treatment

1. Introduction

In recent year, environmental problems caused by dyes from textile and leather industries have the influence on health and hygiene of human due to the high toxicity and high stability under ambient condition [1-4]. The traditional treatment of wastewater including coagulation, ionizing radiation, reverse osmosis, membrane ultrafiltration, adsorption and ion exchange are not suitable for wastewater treatment because they are low efficiency, high cost, non-productive and formation of secondary pollutants [2-7]. Among them, photocatalysis of semiconductor-based photocatalyst is a green technology with cost-effective and economically friendly for degradation of organic pollutants because the organic dyes are completely mineralized into CO_2 and H_2O [3, 5, 8].

ZnO with direct wide band gap of 3.37 eV and large exciton binding energy of ~60 meV is an important member of the II–VI semiconductor which has promising applications for sensors, catalysis, solar cells and optoelectronics [3, 5, 8-10]. It is excellent application in the area of photocatalysis because of its physical and chemical stability, high oxidative capacity, low cost and ease of availability [5, 8-11]. Nevertheless, the photocatalytic application is limited by absorption in the ultraviolet (UV) region and low photonic efficiency [3, 9, 10-12]. Metal doping is the

* Corresponding authors: phuruangrat@hotmail.com
https://doi.org/10.15251/JOR.2024.202.177

effective method to extend photo-response to visible region and suppress the recombination of photo-induced charge carriers of ZnO [3, 8, 11]. Rare earth metals co-doped ZnO is a candidate visible-light-driven photocatalyst because the spectral sensitivity in visible region is extended and charge carrier recombination is suppressed [7, 13-16].

This research is to prepare Ce/Mg co-doped ZnO nanoparticles by the combustion method. Phase, structure, morphology and photocatalytic reaction of Ce/Mg co-doped ZnO nanoparticles were studied and discussed.

2. Experimental details

To prepare ZnO and Ce/Mg co-doped ZnO samples by combustion method, 0.01 mole of $Zn(NO_3)_2 \cdot 6H_2O$ was dissolved in 25 ml of ethanol and followed with the addition of 25 ml ethanol solutions of 0.01–0.02 wt% $Ce(NO_3)_3 \cdot 6H_2O$ and $Mg(NO_3)_2 \cdot 6H_2O$. Then, 0.01 mole of tartaric acid and 0.001 mole NaOH were weighed and dissolved in ethanol. Subsequently, they were added to the solution system under magnetic stirring to form white gel. The white gel was filtered, washed with deionized water and ethanol and dried. The precursor was ground, put in an alumina crucible and calcined in an electric furnace at 600 ºC for 4 h. The final ZnO and Ce/Mg co-doped ZnO samples were analyzed by X-ray diffraction (XRD), transmission electron microscopy (TEM), Fourier transform infrared spectroscopy (FTIR) and Raman spectroscopy.

The photocatalytic performance of ZnO and Ce/Mg co-doped ZnO samples was evaluated through the degradation of methylene blue (MB) illuminated by visible radiation. 200 mg ZnO and Ce/Mg co-doped ZnO samples were suspended in 200 ml of $1x10^{-5}$ M MB solutions. They were stirred in the dark for 30 min and illuminated by visible radiation of a xenon lamp. During visible light illumination, 5 ml of MB solution was withdrawn every 30 min and centrifuged to remove ZnO and Ce/Mg co-doped ZnO residual solid. The concentration of MB was measured at 664 nm by a UV-visible spectrophotometer and the decolorization efficiency was calculated by the below equation.

$$\text{Decolorization efficiency (\%)} = (1 - C_t/C_o)\ x100 \quad (1)$$

C_o and C_t are the initial MB concentration prior to the photocatalytic test and the MB concentration after photocatalytic test for a period of time (t), respectively.

3. Results and discussion

Fig. 1 shows XRD patterns of pure ZnO and $Zn_{0.97}Ce_xMg_{0.03-x}O$ nanoparticles with x = 0.01, 0.015 and 0.02 prepared by combustion method and calcined at 600 ºC for 4 h. All samples were indexed to the hexagonal wurtzite ZnO crystal structure (JCPDS No. 36-1451 [17]). Impurities such as CeO_2 and MgO were not detected in all samples. The dominant diffraction angle of (101) plane of Ce/Mg co-doped ZnO samples was shifted to the lower one because ionic radii of Ce ion (Ce^{3+} = 0.103 nm [15, 18, 19]) and Mg ion (Mg^{2+} = 0.066 nm [20, 21]) are different from Zn ion (Zn^{2+} = 0.074 nm [4, 5, 7, 8, 15]). The XRD results demonstrated that Ce/Mg ions were successfully incorporated in ZnO lattice. The diffraction peaks of Ce/Mg co-doped ZnO samples were broadened, indicating that the degree of crystallinity and crystallite size of Ce/Mg co-doped ZnO samples were reduced as compared to those of pure ZnO sample [5, 8]. The average crystallite sizes of un-doped ZnO and Ce/Mg co-doped ZnO samples were calculated by the Scherrer equation [1, 4, 8, 22, 23]. The calculated crystallite sizes were 33.69, 22.24, 23.49 and 24.90 nm for ZnO, $Zn_{0.97}Ce_{0.02}Mg_{0.01}O$, $Zn_{0.97}Ce_{0.015}Mg_{0.015}O$ and $Zn_{0.97}Ce_{0.01}Mg_{0.02}O$, respectively.

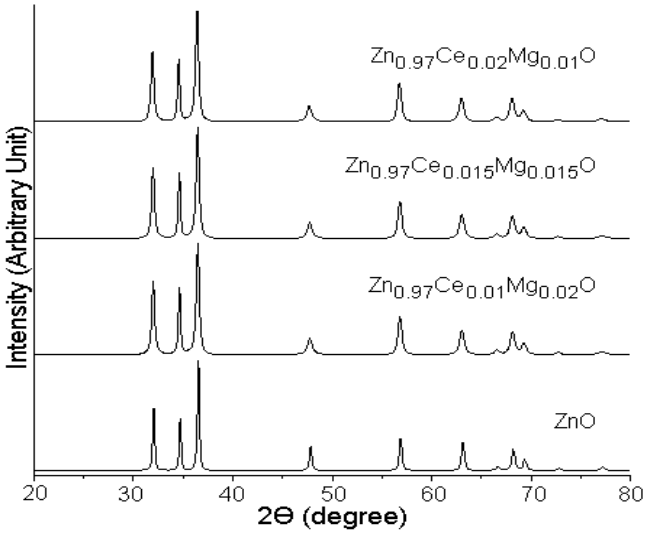

Fig. 1. XRD patterns of ZnO and Ce/Mg co-doped ZnO samples prepared by combustion method and followed by calcination at 600 °C for 4 h.

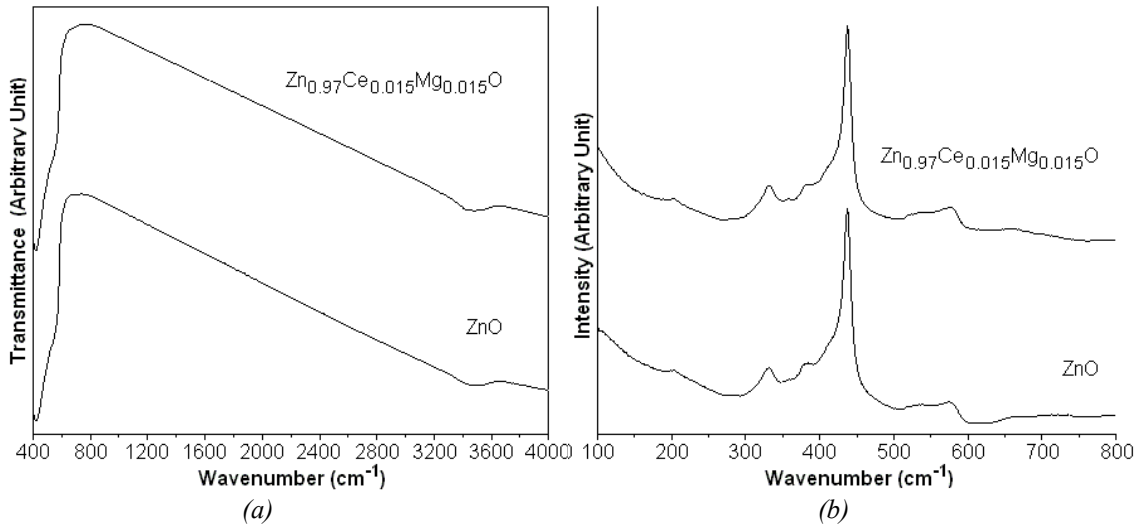

Fig. 2. (a) FTIR and (b) Raman spectra of pure ZnO and $Zn_{0.97}Ce_{0.015}Mg_{0.015}O$ samples prepared by combustion method and calcined at 600 °C for 4 h.

FTIR spectra of pure ZnO and $Zn_{0.97}Ce_{0.015}Mg_{0.015}O$ samples are shown in Fig. 2a. Pure ZnO sample shows the FTIR band at wavenumber of 423 cm^{-1} which indicated the Zn−O stretching mode of hexagonal wurtzite ZnO structure [2, 4, 8, 11, 22]. The wavenumber of Zn–O stretching mode of $Zn_{0.97}Ce_{0.015}Mg_{0.015}O$ nanoparticles was shifted to 420 cm^{-1} caused by the created oxygen defect in the Ce/Mg co-doped ZnO sample [11, 22, 24]. The oxygen defect containing in Ce/Mg co-doped ZnO sample acted as an electron acceptor which suppressed electron-hole recombination during photocatalytic process and improved the photocatalytic activity [18, 14, 25, 26]. The broad bands around 3350 cm^{-1} were detected in both samples and correspond with the OH stretching vibration of adsorbed water on the samples [2, 4, 5, 8, 22].

Raman spectra of ZnO and $Zn_{0.97}Ce_{0.015}Mg_{0.015}O$ samples are shown in Fig. 2b. The sharp Raman peak of ZnO nanoparticles at 439 cm^{-1} corresponds to the optical phonon E_{2H} mode of typical characteristic wurtzite ZnO structure [8, 22, 27]. The nonpolar optical phonon E_{2H} and A_1(TO) modes of wurtzite ZnO structure were detected at 414 and 382 cm^{-1} [8, 22, 27]. Two weak Raman peaks at 200 and 331 cm^{-1} were detected in the spectrum of pure ZnO nanoparticles and

were attributed to E_{2L} and E_{2H}–E_{2L} modes [8, 22, 28]. The shoulder at 535 cm^{-1} was attributed to the A_1(LO) mode [8, 22, 27]. In addition, E_1(LO) mode of wurtzite ZnO structure related to the impurities containing in ZnO lattice such as oxygen vacancies and zinc interstitials was detected at 575 cm^{-1} [8, 22, 27]. Moreover, the intensity of A_1(LO) mode of $Zn_{0.97}Ce_{0.015}Mg_{0.015}O$ sample is higher than that of pure ZnO sample because more defects were created in ZnO lattice by doping process [8, 22, 28, 29].

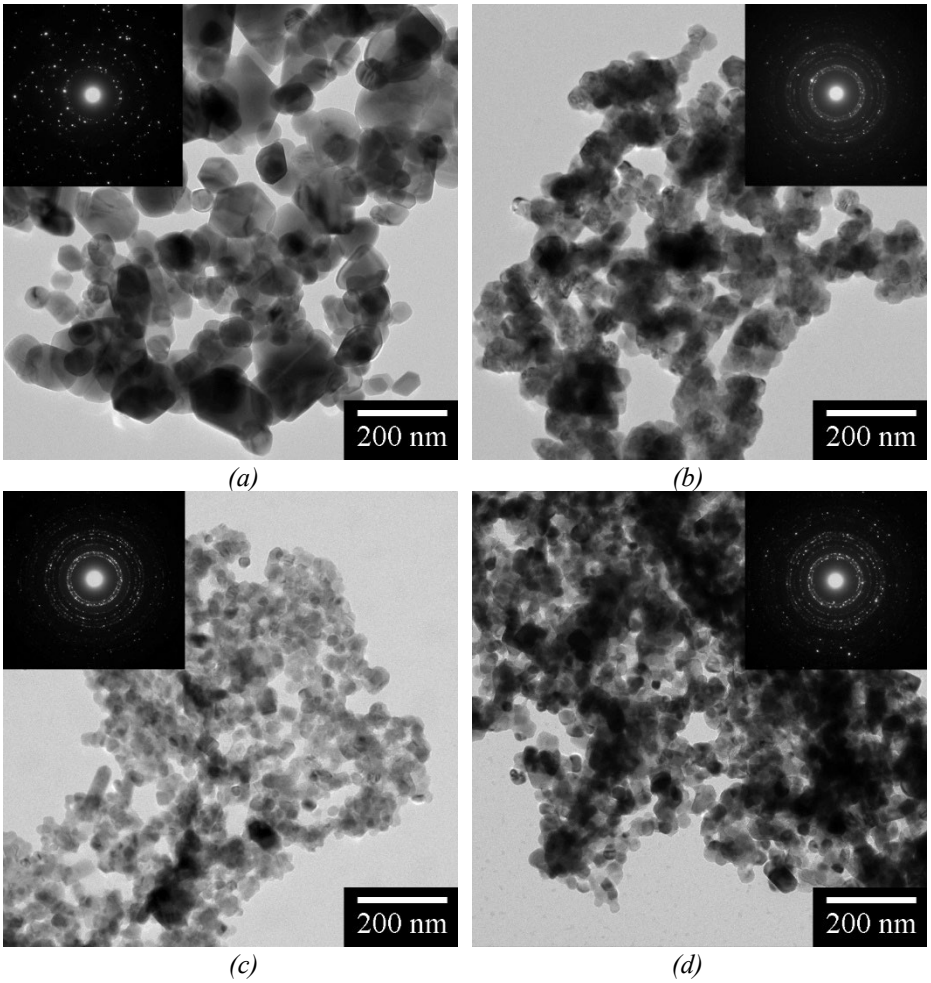

Fig. 3. TEM images and SAED patterns of (a) ZnO, (b) $Zn_{0.97}Ce_{0.02}Mg_{0.01}O$, (c) $Zn_{0.97}Ce_{0.015}Mg_{0.015}O$ and (d) $Zn_{0.97}Ce_{0.01}Mg_{0.02}O$ nanoparticles prepared by combustion method and calcined at 600 °C for 4 h.

Fig. 3 exhibits the TEM images of pure ZnO and $Zn_{0.97}Ce_xMg_{0.03-x}O$ (x = 0.01, 0.015 and 0.02) nanoparticles with calcination at 600 °C for 4 h. TEM images of pure ZnO and Ce/Mg co-doped ZnO samples show that the products were composed of spherical nanoparticles with different orientations. They were pure ZnO and Ce/Mg co-doped ZnO with uniformly and homogeneously distributed nanoparticles. Fig. 4 shows the particle size distribution of pure ZnO and Ce/Mg co-doped ZnO samples of 200 counted particles from the corresponding TEM images. The particle size distribution histogram of pure ZnO sample contained particle size of 40–220 nm with average particle size of 92.15 ± 32.69 nm. The particle size distributions of as-synthesized Ce/Mg co-doped ZnO samples were in the range of 30–75, 20–45 and 15–60 nm for $Zn_{0.97}Ce_{0.02}Mg_{0.01}O$, $Zn_{0.97}Ce_{0.015}Mg_{0.015}O$ and $Zn_{0.97}Ce_{0.01}Mg_{0.02}O$, respectively. The average particle sizes of Ce/Mg co-doped ZnO samples were 45.30 ± 7.87, 27.98 ± 4.96 and 36.85 ± 7.38 nm for $Zn_{0.97}Ce_{0.02}Mg_{0.01}O$, $Zn_{0.97}Ce_{0.015}Mg_{0.015}O$ and $Zn_{0.97}Ce_{0.01}Mg_{0.02}O$, respectively. In this

research, the Ce/Mg dopant in ZnO lattice played the role in inhibiting growth rate of ZnO nanoparticles because movement of grain boundaries of the nanoparticles was resisted. Higher active surface area for production of active radicals for dye degradation was produced. These results can lead to improve the photodegradation of dye [4, 7, 11, 15, 22, 30]. The selected area electron diffraction (SAED) patterns of ZnO and Ce/Mg co-doped ZnO nanoparticles (Fig. 3 (inset)) appeared as diffraction rings which were indexed to pure phase of hexagonal wurtzite ZnO crystal.

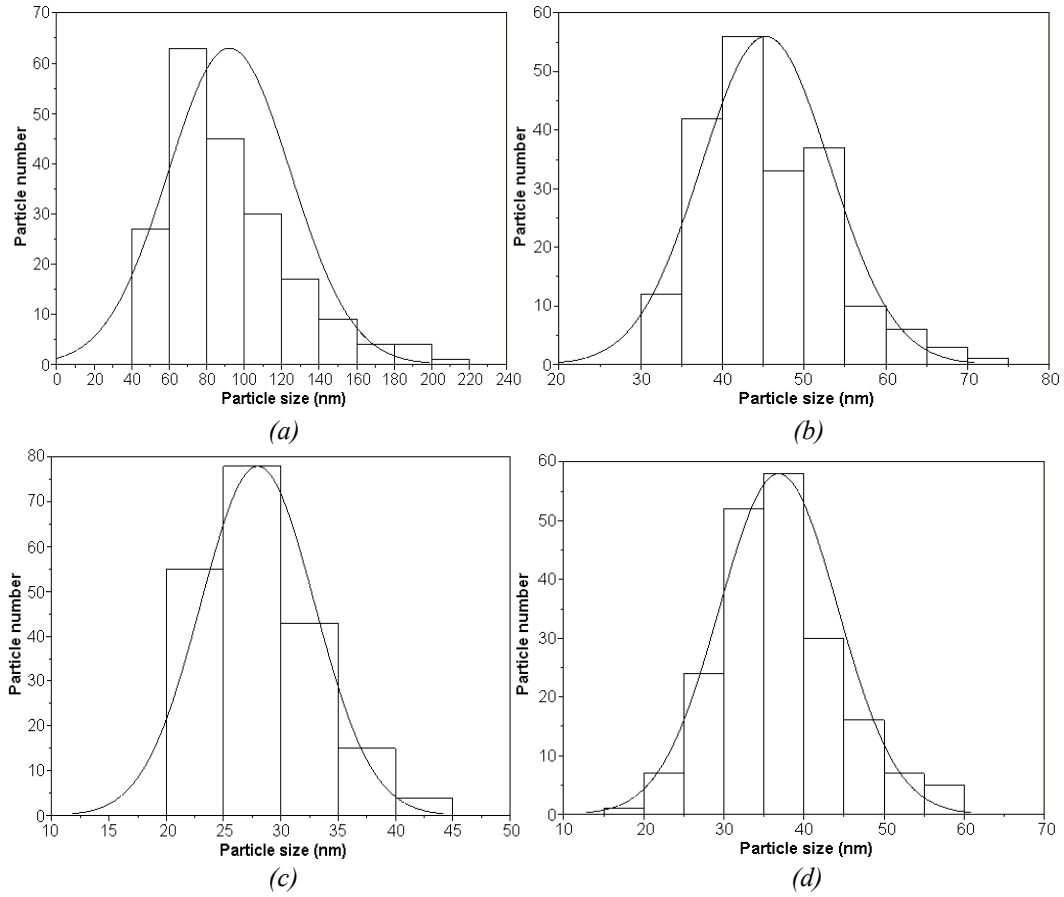

Fig. 4. Particle size distributions of (a) ZnO, (b) $Zn_{0.97}Ce_{0.02}Mg_{0.01}O$, (c) $Zn_{0.97}Ce_{0.015}Mg_{0.015}O$ and (d) $Zn_{0.97}Ce_{0.01}Mg_{0.02}O$ nanoparticles prepared by combustion method and calcined at 600 °C for 4 h.

Fig. 5a exhibits photodegradation of MB over pure ZnO and $Zn_{0.97}Ce_xMg_{0.03-x}O$ nanoparticles with x = 0.01, 0.015 and 0.02 under visible light irradiation. The pure ZnO nanoparticles have the photodegradation efficiency under visible light irradiation of 21.44% within 150 min. The photodegradation efficiencies were increased when Ce/Mg nanoparticles were doped in ZnO lattice. Among these samples, the $Zn_{0.97}Ce_{0.015}Mg_{0.015}O$ nanoparticles have the highest MB degradation performance of 95.16% (4.44 times the MB degradation photocatalyzed by pure ZnO) within 150 min because the highest photocatalytic performance of the Ce/Mg co-doped ZnO sample mainly attributed to the largest specific surface area, smallest crystallite size and highest visible light absorption capacity [4, 7, 8, 22, 30]. The degradation rates for the pure ZnO and Ce/Mg co-doped ZnO nanoparticles were studied and fitted to the below pseudo-first-order equation.

$$\ln (C_o/C_t) = k_{app}t \quad (2)$$

, where k_{app} is the apparent rate constant [1, 3, 4, 8, 15, 22, 30, 31]. Fig. 5b shows the linear plotted lines for photocatalytic degradation of MB over pure ZnO and Ce/Mg co-doped ZnO under visible

light irradiation. The kinetic rate constants of photocatalysis were $1.51x10^{-3}$, 0.0156, 0.0189 and 0.0129 min^{-1} for pure ZnO, $Zn_{0.97}Ce_{0.02}Mg_{0.01}O$, $Zn_{0.97}Ce_{0.015}Mg_{0.015}O$ and $Zn_{0.97}Ce_{0.01}Mg_{0.02}O$ nanoparticles, respectively. Clearly, $Zn_{0.97}Ce_{0.015}Mg_{0.015}O$ nanoparticles have the highest apparent rate constant.

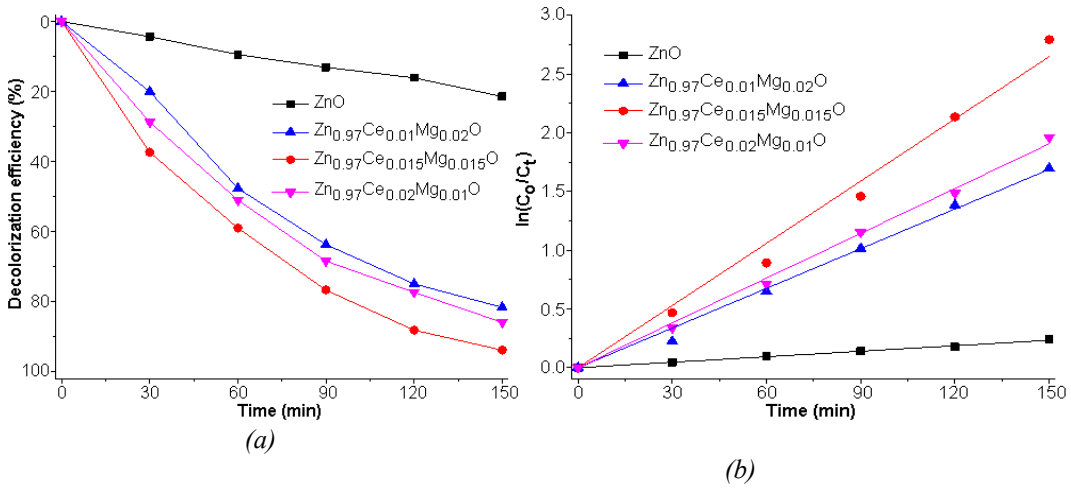

Fig. 5. (a) Decolorization efficiencies and (b) pseudo-first-order plots for MB degradation over ZnO and Ce/Mg co-doped ZnO nanoparticles under visible light irradiation.

The stability of reused $Zn_{0.97}Ce_{0.015}Mg_{0.015}O$ nanoparticles was tested by MB degradation for five cycles as the results shown in Fig. 6a. The photodegradation efficiency for MB in the presence of $Zn_{0.97}Ce_{0.015}Mg_{0.015}O$ nanoparticles at the conclusion of the 5th cycle was decreased to 88.32%. This test proves that $Zn_{0.97}Ce_{0.015}Mg_{0.015}O$ nanoparticles are highly stable and reusable under visible light irradiation. In addition, the reactive species for photocatalytic reaction of $Zn_{0.97}Ce_{0.015}Mg_{0.015}O$ nanoparticles were determined by the addition of ethylenediaminetetraacetic acid disodium (EDTA-2Na), isopropyl alcohol (IPA) and benzoquinone (BQ) for scavenging hole (h^+), hydroxyl radical ($^{\bullet}OH$) and superoxide anion ($^{\bullet}O_2^-$) containing in the solution system, respectively (Fig. 6b) [1, 4, 11, 22, 32]. The results show that the photodegradation efficiencies of $Zn_{0.97}Ce_{0.015}Mg_{0.015}O$ nanoparticles in the solution system containing IPA and BQ were decreased to 10.35% and 36.4%, respectively. Clearly, both $^{\bullet}OH$ and $^{\bullet}O_2^-$ were the main active species for MB degradation photocatalyzed by $Zn_{0.97}Ce_{0.015}Mg_{0.015}O$ nanoparticles under visible light irradiation [4, 22, 32]. Meanwhile, the photocatalytic degradation of MB was little suppressed by the addition of EDTA-2Na. Thus, h^+ was the minor active species for MB degradation [4, 22, 32].

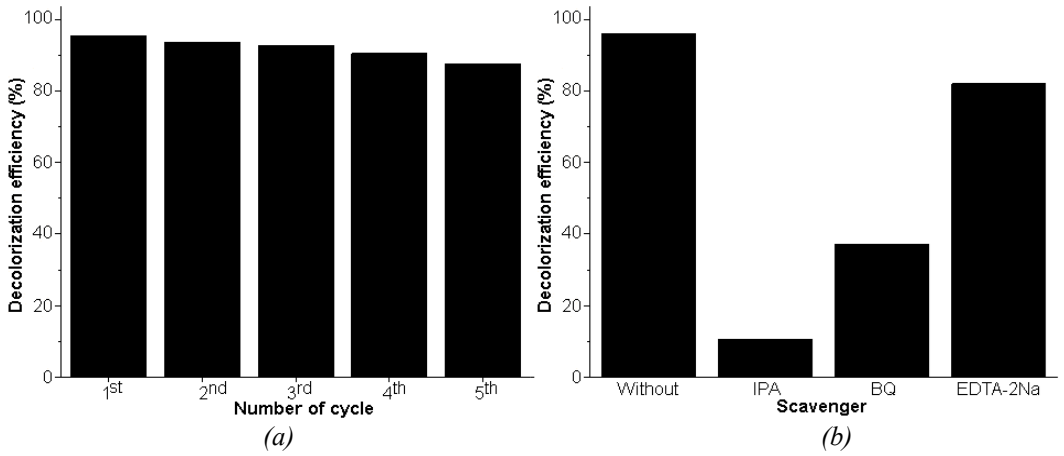

Fig. 6. (a) The stability test and (b) scavenger test for MB degradation over $Zn_{0.97}Ce_{0.015}Mg_{0.015}O$ nanoparticles under visible light irradiation.

Fig. 7 shows a proposed mechanism for photocatalysis of Ce/Mg co-doped ZnO nanoparticles in the degradation of MB under visible light irradiation. The Ce/Mg co-dopant created a shallow donor level inside band gap energy which captured electrons and prevented electron-hole recombination [14, 33, 34]. The $Zn_{0.97}Ce_xMg_{0.03-x}O$ nanoparticles absorbed photon (quantized particle) and excited electrons to reside in conduction band, including the induction of holes (h^+_{VB}) in valence band [4, 6, 8]. The electrons on the surface of $Zn_{0.97}Ce_xMg_{0.03-x}O$ nanoparticles reacted with dissolved oxygen (O_2) to produce superoxide anion ($^\bullet O_2^-$). Meanwhile, the induced holes combined with water (H_2O)/hydroxide (OH^-) ion to produce hydroxyl radical ($^\bullet OH$) [4, 6, 8]. In addition, $^\bullet O_2^-$, $^\bullet OH$ and h^+_{VB} were able to directly transform MB into H_2O and CO_2 [4, 6, 8]. The photocatalytic mechanism of $Zn_{0.97}Ce_xMg_{0.03-x}O$ nanoparticles in degrading MB under visible light irradiation can be described as follows [4, 6, 8, 16].

$$Zn_{0.97}Ce_xMg_{0.03-x}O + h\nu \rightarrow e^-_{CB} + h^+_{VB} \quad (3)$$

$$e^-_{CB} + O_2 \rightarrow {}^\bullet O_2^- \quad (4)$$

$$h^+_{VB} + OH^-/H_2O \rightarrow {}^\bullet OH \quad (5)$$

$$^\bullet O_2^-/{}^\bullet OH + MB \rightarrow CO_2 + H_2O \quad (6)$$

$$h^+_{VB} + MB \rightarrow CO_2 + H_2O \quad (7)$$

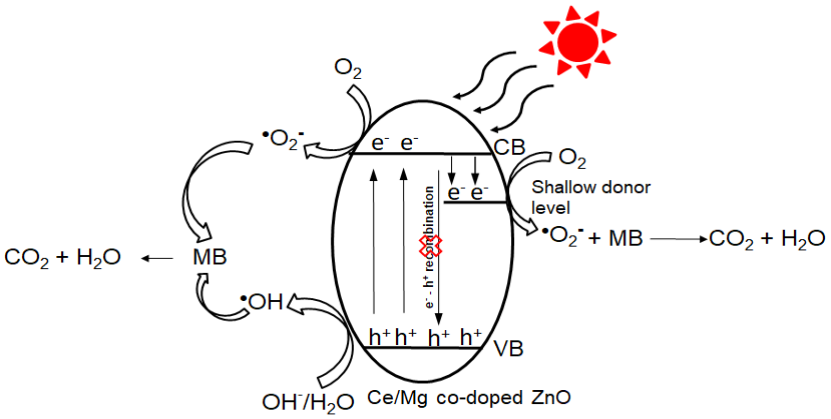

Fig. 7. Schematic illustration for photocatalysis of Ce/Mg co-doped ZnO nanoparticles under visible light irradiation.

4. Conclusions

In this research, as-synthesized Ce/Mg co-doped ZnO nanoparticles were synthesized by combustion method for MB gradation under visible light irradiation. The analytical results show that the as-synthesized Ce/Mg co-doped ZnO samples were pure phase of hexagonal wurtzite ZnO nanoparticles. Among the different samples, the $Zn_{0.97}Ce_{0.015}Mg_{0.015}O$ nanoparticles have the highest MB degradation performance of 4.44 times the MB photodegradation catalyzed by pure ZnO nanoparticles and were reusable for 5 recycle runs under visible light irradiation.

Acknowledgements

This research was supported by National Science, Research and Innovation Fund (NSRF) and Prince of Songkla University (Grant No. SCI6701034S).

References

[1] X. Chen, Z. Wu, D. Liu, Z. Gao, Nanoscale Res. Lett. 12, 143 (2017); https://doi.org/10.1186/s11671-017-1904-4
[2] S. Rabieh, K. Nassimi, M. Bagheri, J. Mater. Sci. 27, 10052–10058 (2016); https://doi.org/10.1007/s10854-016-5077-1
[3] D. Zhang, F. Zeng, J. Mater. Sci. 47, 2155–2161 (2012); https://doi.org/10.1007/s10853-011-6016-4
[4] D. Laokae, A. Phuruangrat, T. Thongtem, S. Thongtem, Russ. J. Inorg. Chem. 67, 721–731 (2022); https://doi.org/10.1134/S0036023622050114
[5] C. Kuang, P. Tan, A. Bahadur, S. Iqbal, M. Javed, M.A. Qamar, M. Fayyaz, G. Liu, O.M. Alzahrani, E. Alzahrani, A.E. Farouk, J. Mater. Sci. 33, 9930–9940 (2022); https://doi.org/10.1007/s10854-022-07984-6
[6] R.R. Chandrapal, S. Bharathkumar, G. Bakiyaraj, V. Ganesh, J. Archana, M. Navaneethan, Appl. Nanosci. 12, 1869–1884 (2022); https://doi.org/10.1007/s13204-022-02414-9
[7] B. Khanizadeh, M. Khosravi, M.A. Behnajady, A. Shamel, B. Vahid, Period. Polytech. Chem. Eng. 64, 61–74 (2020); https://doi.org/10.3311/PPch.12959
[8] S. Sa-nguanprang, A. Phuruangrat, T. Thongtem, S. Thongtem, Russ. J. Inorg. Chem. 64, 1600–1608(2019); https://doi.org/10.1134/S0036023619120143
[9] B.M. Rajbongshi, A. Ramchiary, B.M. Jha, S.K. Samdarshi, J. Mater. Sci. 25, 2969–2973 (2014); https://doi.org/10.1007/s10854-014-1968-1
[10] T. Chankhanittha, J. Watcharakitti, S. Nanan, J. Mater. Sci. 30, 17804–17819 (2019); https://doi.org/10.1007/s10854-019-02132-z
[11] N. Elamin, A. Modwi, M.A. Ben Aissa, K.K. Taha, O.K. Al-Duaij, T.A. Youse, J. Mater. Sci. 32, 2234–2248 (2021); https://doi.org/10.1007/s10854-020-04988-y
[12] J. Liu, Z. Shi, X. Li, J. Yang, J. Lang, J. Mater. Sci. 30, 13690–13697 (2019); https://doi.org/10.1007/s10854-019-01746-7
[13] U. Alam, A. Khan, W. Raza, A. Khan, D. Bahnemann, M. Muneer, Catal. Today 284, 169-178 (2017); https://doi.org/10.1016/j.cattod.2016.11.037
[14] N.Q. Yang, J. Li, Y.N. Wang, J. Ma, Mater. Sci. Semicond. Process. 131, 105835 (2021); https://doi.org/10.1016/j.mssp.2021.105835
[15] I. Ahmad, M.S.b Akhtar, E. Ahmed, M. Ahmad, J. Rare Earths 39, 151-159 (2021); https://doi.org/10.1016/j.jre.2019.11.006
[16] S. Benzitouni, M. Zaabat, M.S. Aida, J. Ebothe, J. Michel, B. Boudine, L. Mansouri, T. Saidani, Optik 156, 949–960 (2018); https://doi.org/10.1016/j.ijleo.2017.12.039
[17] Powder Diffract. File, JCPDS-ICDD, 12 Campus Blvd., Newtown Square, PA 19073-3273, U.S.A. (2001).
[18] N.F. Djaja, R. Saleh, Materials Sciences and Applications 4, 145-152 (2013); http://dx.doi.org/10.4236/msa.2013.42017
[19] I.V. Zagaynov, E.Y. Liberman, J. Chem. Sci. 128, 861–865 (2016); https://doi.org/10.1007/s12039-016-1101-5
[20] N. Kılınç, L. Arda, S. Öztürk, Z.Z. Öztürk, Cryst. Res. Technol. 45, 529-538 (2010); https://doi.org/10.1002/crat.200900662
[21] Y.J. Yun, H.J. Lim, J.S. Park, M. Wu, H.K. Jung, S. Choi, Dalton Trans. 44, 338-344 (2015); https://doi.org/10.1039/c4dt02457e
[22] A. Phuruangrat, T. Thongtem, S. Thongtem, Dig. J. Nanomater. Bios. 18, 1423-1431 (2023); https://doi.org/10.15251/DJNB.2023.184.1423
[23] M.S. Viswaksenan, A. Simi, A. Panneerselvam, Dig. J. Nanomater. Bios. 18, 859- 868 (2023); https://doi.org/10.15251/DJNB.2023.183.859
[24] F. Adam, A. Himawan, M. Aswad, D. Tahir, IOP Conf. Series: J. Phys.: Conf. Ser. 1317, 012051 (2019); https://doi.org/10.1088/1742-6596/1317/1/012051
[25] Y. Yu, B. Yao, Y. He, B. Cao, W. Ma, L. Chang, Mater. Chem. Phys. 244, 122672 (2020); https://doi.org/10.1016/j.matchemphys.2020.122672
[26] T.V.H. Luu, N.N. Dao, H.A.L. Pham, Q.B. Nguyen, V.C. Nguyen, P.H. Dang, RSC Adv., 13,

5208-5218 (2023); https://doi.org/10.1039/d2ra07655a
[27] A.S. Nazir, Z. Imran, A. Malik, M. Nazir, M.W. Ashraf, S. Tayyaba, Digest Journal of Nanomaterials and Bios. 13, 307-313 (2018).
[28] V. Tiron, I.L. Velicu, D. Stanescu, H. Magnan, L. Sirghi, Surf. Coat. Tech. 324, 594-600 (2017); http://dx.doi.org/10.1016/j.surfcoat.2016.11.087
[29] J.Z. Marinho, L.F. de Paula, E. Longo, A.O.T. Patrocinio, R.C. Lima, SN Appl. Sci. 1, 359 (2019); https://doi.org/10.1007/s42452-019-0359-x
[30] P. Patiphatpanya, P. Intaphong, A. Phuruangrat, B. Kuntalue, P. Dumrongrojthanath, T. Thongtem, S. Thongtem, Dig. J. Nanomater. Bios. 15, 115-121 (2020).
[31] G. Murugadoss, M. R. Kumar, A. Kathalingam, J. R. Rajabathar, H. Al-Lohedan, D. M. Al-Dhayan, J. Ovonic Res. 17, 595-603 (2021).
[32] A. Phuruangrat, S. Thamsukho, S. Thungprasert, T. Sakhon, T. Thongtem, S. Thongtem, J. Ovonic Res. 18, 149-158 (2022); https://doi.org/10.15251/JOR.2022.182.149
[33] A. Samanta, M.N. Goswami, P.K. Mahapatra, Mater. Res. Express 6, 065031 (2019); https://doi.org/10.1088/2053-1591/ab0c25
[34] I. Ahmad, M. E. Mazhar, M. N. Usmani, K. Khan, S. Ahmad, J. Ahmad, J. Ovonic Res. 15, 1-13 (2019).